

14. M. R. Weaver, D. Abraham, *J. Vac. Sci. Technol. B* **9**, 1559 (1991).
15. The quick variation of the electrostatic forces cannot be followed by the distance-controlling feedback, which keeps the mean value of the total normal force constant over several lattice constants.
16. T. Schimmel *et al.*, Eds. *Forces in Scanning Probe Methods* (North Atlantic Treaty Organization–Advanced Study Institute Series, Kluwer, Dordrecht, Netherlands, 1995).
17. J. Kerssemakers, J. T. M. De Hosson, *Surf. Sci.* **417**, 281 (1998).
18. F. Dinelli, S. K. Biswas, G. A. D. Briggs, O. V. Kolosov, *Appl. Phys. Lett.* **71**, 1177 (1997).
19. M. Heuberger, C. Drummond, J. Israelachvili, *J. Phys. Chem. B* **102**, 5038 (1998).
20. L. Bureau, T. Baumberger, C. Caroli, *Phys. Rev. E* **62**, 6810 (2000).
21. J. P. Gao, W. D. Luedtke, U. Landman, *J. Phys. Chem. B* **102**, 5033 (1998).
22. V. Zaloj, M. Urbakh, J. Klafter, *Phys. Rev. Lett.* **82**, 4823 (1999).
23. M. G. Rozman, M. Urbakh, J. Klafter, *Phys. Rev. E* **57**, 7340 (1998).
24. E. Riedo, E. Gnecco, R. Bennewitz, E. Meyer, H. Brune, *Phys. Rev. Lett.* **91**, 084502 (2003).
25. This work was supported by the Swiss National Science Foundation, the National Center of Competence in Research on Nanoscale Science, the Kommission zur Förderung von Technologie und Innovation, and the European Science Foundation Nanotribo program. M. T. Cuberes is gratefully acknowledged for discussions and advice.

6 February 2006; accepted 25 May 2006  
10.1126/science.1125874

## Dynamic Forces Between Two Deformable Oil Droplets in Water

Raymond R. Dagastine,<sup>1,2</sup> Rogério Manica,<sup>1,3</sup> Steven L. Carnie,<sup>1,3</sup> D. Y. C. Chan,<sup>1,3</sup> Geoffrey W. Stevens,<sup>1,2</sup> Franz Grieser<sup>1,4\*</sup>

The understanding of static interactions in colloidal suspensions is well established, whereas dynamic interactions more relevant to biological and other suspended soft-matter systems are less well understood. We present the direct force measurement and quantitative theoretical description for dynamic forces for liquid droplets in another immiscible fluid. Analysis of this system demonstrates the strong link between interfacial deformation, static surface forces, and hydrodynamic drainage, which govern dynamic droplet-droplet interactions over the length scale of nanometers and over the time scales of Brownian collisions. The results and analysis have direct bearing on the control and manipulation of suspended droplets in soft-matter systems ranging from the emulsions in shampoo to cellular interactions.

Much of the ability to produce advanced materials relies on a well-developed understanding of surface forces. Static interactions between surfaces have been studied for decades (1–3), but a comprehensive quantitative understanding of dynamic interactions in biological and other suspended soft-matter systems is still being developed. These dynamic forces are the basis behind manipulating and controlling soft-matter systems, such as complex fluids or emulsions, in formulation and processing. The challenge in understanding lies in both the quantitative measurement and the ability to predict dynamic droplet-droplet interactions, which are more complicated than the analogs in solid particulate suspensions. The experimental and theoretical analyses presented in this work describe the dynamic interactions between two deformable oil droplets. The general methodology presented in this study is applicable to all soft-matter systems and opens another dimension to the observable forces in collisions arising from Brownian motion.

The interactions between droplets common to emulsions with droplet radii, between 10 and 100  $\mu\text{m}$ , have been difficult to measure experi-

mentally. Atomic force microscopy (AFM) has been used to examine the equilibrium interactions between a rigid probe particle and a single bubble or droplet in this size range (4–6). In addition, one study has examined the hydrodynamic interaction between a single oil droplet and a rigid probe particle with a semiquantitative analysis (7). However, these studies lack a specific relevance to the dynamic interactions between soft matter, such as emulsion droplets, where every interface is deformable. Recent developments have allowed for direct force measurement of the interactions between droplets with radii of the order of 40  $\mu\text{m}$  (8) and the development of a quantitative model for these systems (9, 10). By comparing the model to experimental observations on these intermediate-size drops, this study has developed an understanding of dynamic droplet-droplet interactions in a region where deformation, hydrodynamic drainage, and interaction forces are all important.

The droplet size range in this study is bracketed by droplet sizes that have largely decoupled deformation, surface forces, and hydrodynamic drainage effects. For droplet radii below 10  $\mu\text{m}$ , the droplet internal pressure is large enough that equilibrium surface forces dominate the interaction over deformation and hydrodynamic effects. For droplet radii above 100  $\mu\text{m}$ , there is a large body of work that uses interferometry to measure interfacial profiles, with time (11) between approaching capillaries at either constant velocity (12) or constant force

(13). The deformation and hydrodynamic drainage effects in this larger droplet regime are mostly decoupled from equilibrium surface forces in a two-stage process (14). The results of the present study provide considerable insight into how to quantitatively model droplet-droplet interactions for this intermediate droplet size and, more important, how the traditional concepts of drainage as a two-stage process are not appropriate for droplet sizes relevant to real emulsions. This may have considerable implications with respect to improving the design and operation of emulsion processing equipment.

Two decane droplets with radii of 43 and 90  $\mu\text{m}$ , in solutions of an anionic surfactant, sodium dodecyl sulfate (SDS), and 1 mM sodium nitrate, were immobilized on an AFM cantilever and substrate (Fig. 1A). The dynamic interaction force between these oil droplets as a function of piezo drive motion of the substrate for a series of approach and retract velocities of the piezo actuator is shown in Fig. 1, B to D. The SDS adsorbed at the oil-water interface controls both the interfacial tension and the surface charge at the interface, where both of these effects are well characterized for the decane-SDS-water system (15). It is not possible to decouple interfacial deformation and separation distance from these data without interpretation through modeling. Therefore, it is standard practice to assign an arbitrary origin for piezo motion; in this case, the origin is set at the highest measured force (16, 17).

The approach and subsequent retracting curves show a strong dependence on the piezo velocity. The approach curves show a hydrodynamic repulsion due to film drainage between the surfaces with a dynamic behavior slower than the time scale of the measurement. The magnitude of the attractive well in the retracting curve is a function of velocity. The time required for the oil droplets to restore upon retraction is a result of the fluid film thickening and the pressure profile between the droplets resisting fluid flow on a time scale longer than the time scale of the measurement. The velocity range spans the likely velocities of an emulsion droplet of comparable size undergoing Brownian motion. For example, the root mean square velocity due to Brownian motion of an oil droplet with a radius of 40  $\mu\text{m}$  is

<sup>1</sup>Particulate Fluids Processing Center, <sup>2</sup>Department of Chemical and Biomolecular Engineering, <sup>3</sup>Department of Mathematics and Statistics, <sup>4</sup>School of Chemistry, University of Melbourne, Victoria 3010, Australia.

\*To whom correspondence should be addressed. E-mail: franz@unimelb.edu.au

approximately 7  $\mu\text{m/s}$  in water at room temperature (9). The measurements demonstrate that hydrodynamic interactions between droplets in this size range are not insignificant even when describing emulsion stability, where equilibrium forces are commonly assumed to dominate.

A quantitative analysis of these data and determination of the interfacial separation require development of an approach based on the augmented Young-Laplace equation and the methods developed for static or equilibrium force measurements between a rigid particle and droplet (17) or between two droplets (18). The dynamic problem contains three disparate length scales: the droplet radii, on the order of 50  $\mu\text{m}$ ; the axial length scale of the interaction forces, from 10 to 100 nm; and the radial length scale of the interaction, on the order of 1 to 5  $\mu\text{m}$ . A more robust model is required to treat these disparate length scales and incorporate the static forces with the hydrodynamic drainage behavior at a deformable interface (7, 9, 10). The lubrication approximation is used to describe the forces across the thin film between the droplets and neglects the hydrodynamic drag on the droplet outside this lateral interaction area. This requires low capillary numbers ( $Ca = \mu V/\sigma$ ), which span  $10^{-6}$  to  $10^{-8}$  for this system, where  $V$  is the droplet velocity,  $\sigma$  is the interfacial tension, and  $\mu$  is the viscosity.

The two main coupled partial differential equations are the standard Reynolds drainage equation and the normal stress balance:

$$\frac{\partial h}{\partial t} = \frac{1}{12\mu r} \frac{\partial}{\partial r} \left( rh^3 \frac{\partial p}{\partial r} \right)$$

$$p + P(h) = \frac{2s}{R_0} - \frac{2s}{r} \frac{\partial}{\partial r} \left( r \frac{\partial h}{\partial r} \right) \quad (1)$$

where  $h(r,t)$  is the interdroplet separation,  $p$  is the hydrodynamic pressure,  $\Pi$  is the equilibrium disjoining pressure, and  $R_0$  is the harmonic mean of the unperturbed droplet radii on the cantilever,  $R_1$ , and the substrate,  $R_2$ . The position of the interfacial profile must be calculated for each droplet. A no-slip boundary condition is employed at the aqueous solution–oil interface for the drainage between the droplets in the presence of surfactant, SDS. This assumption is supported by a number of theoretical and experimental studies (15, 19, 20) that suggest that the adsorption of surfactant molecules on the interface is sufficient to arrest momentum transfer across the interface and prevent any internal flow in the droplets.

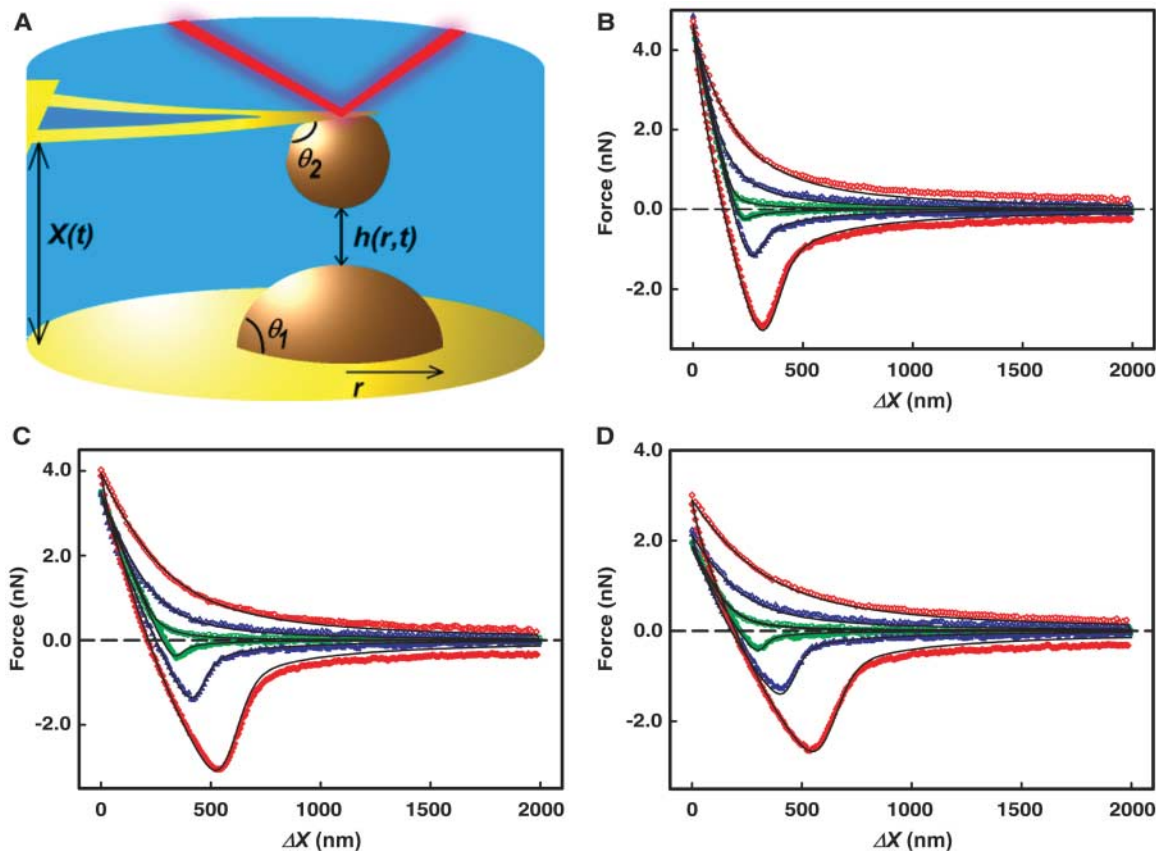
This study differs from previous work in two respects. First, one droplet is immobilized on a cantilever that has an added degree of freedom and that must be incorporated into the drainage equations (9, 10). Second, the treatment of the boundary conditions for the velocity of the interface at large radial distances is far more rigorous in accounting for changes in inter-

facial deformation. The traditional approach assumes that the velocity matches the velocity of the drive actuator (in this case, the piezo) at a large radial distance,  $r_{\text{max}}$ , where the interaction forces are insignificant (12, 20). The previous studies do not account for the constant volume constraint of the droplet in the velocity calculation. A dynamic interaction results in a time-dependent deformation of the droplet's inner region, which results in a time-dependent bulge of the droplet's outer region and changes the velocity at  $r_{\text{max}}$  (9, 10). Details on the calculations, methods, and boundary conditions are presented elsewhere (21).

For a comparison of experimental data of the AFM measurable quantities, force and piezo drive motion, with theoretical calculations, several independently measured experimental parameters are required, including the interfacial tension and the contact angles of the droplets on the piezo drive and the cantilever (21). The disjoining pressure for this system was calculated on the basis of the numerical solution to the Poisson-Boltzmann equation to describe the electrostatic double-layer repulsion between the negatively charged surfactant-laden interfaces. The surface potential required for this calculation was previously measured for the decane-SDS-water system to be  $-100$  mV from an electrokinetic study (15).

The comparison of the model output and the experimental data is shown in Fig. 1, B to D. The one parameter determined from the fit of the

**Fig. 1.** (A) A schematic of the experiment between two oil droplets, one immobilized on the cantilever and the other immobilized on the substrate of an atomic force microscope. (B to D) The dynamic interaction force  $F$  versus piezo drive motion  $\Delta X$  between two decane droplets in aqueous solution in the presence of SDS at a series of approach (open symbols) and retract (filled symbols) velocities (green circles, 2  $\mu\text{m/s}$ ; blue triangles, 9.3  $\mu\text{m/s}$ ; red diamonds, 28  $\mu\text{m/s}$ ) over a range of SDS concentrations: (B) 0.1 mM, (C) 3 mM, and (D) 10 mM. The points refer to the experimental data, and the solid lines are the calculated force curves from a comprehensive model of the dynamic droplet interactions.



model to the data is the only unknown in the system, the initial starting separation distance  $h_0$ . Each force curve is an independent measurement, and the starting distances vary from 20 to 50 nm at a given SDS concentration, as shown in Fig. 1, B to D, where the total piezo drive is 2  $\mu\text{m}$  and  $h_0$  ranges from 1.75  $\mu\text{m}$  to 1.89  $\mu\text{m}$ . A sensitivity study shown in fig. S1 demonstrates that a 100-nm change in initial starting distance results in a 20% change in the maximum measured force and the position of the minimum. This analysis leads to a resolution in the determined distance of  $\sim 20$  nm over 2  $\mu\text{m}$ , or an accuracy better than 1% in separation.

Although the agreement is notable, a discussion of the impact of the experimental error on the comparison with the theory is warranted. The independently measured parameters mentioned above all have an experimental uncertainty, but the largest source of error on these force data is the experimental error in the calibration of the cantilever spring, constant with an accuracy of 10% (22). A sensitivity study has shown that the theory is sensitive to statistically significant errors in each of the above parameters, but a comparison of the impact of all these errors on the theoretical calculations offers a more practical comparison to the experimental data. The gray regions in Fig. 2, A and B, are bounded by the maximum and minimum experimental uncertainties for all these parameters for a velocity of 28  $\mu\text{m/s}$ . The agreement shown for the 3 mM SDS case is typical for all the concentrations and velocities where the experimental data are centered on the theoretical predictions. The only exception is the 10 mM case, where the data are on the edge of the parameter bounds. The critical micelle concentration for SDS is approximately 8 mM. The disjoining pressure calculation only accounts for the effect of micelles on the solution ionic strength and not any possible additional effect on the disjoining pressure.

Two features of these force data can now be explained by using the validated model to develop a larger understanding of what occurs at the interface during the drainage process. First, drop coalescence caused by an ever-present van der Waals force is not observed, even though a significant attractive force is observed between these droplets. Second, the smoothly varying minima exhibit a strong dependence on the approach and retract velocities.

It has been shown for the static interactions for these droplet sizes that repulsive forces are always observed experimentally for all SDS concentrations (18). Modeling of the static system has shown that the interface flattens at the radial center of the film as the interdroplet disjoining pressure approaches the Laplace pressure of the droplets (18). The phenomenon limits to a finite separation distance according to the relation  $\Pi(h_l) = 2\sigma/R_0$ , where  $h_l$  is this limiting distance, which is commonly on the order of nanometers for the experimental sys-

tems studied (18). For this static system, the limiting distance is always larger than the length scale of the van der Waals attraction; therefore, attraction is never observed. For the dynamic

case, the flattening of the droplet occurs on the approach curve whenever the normal pressure is on the order of the droplet Laplace pressure, regardless of the contribution to the pressure

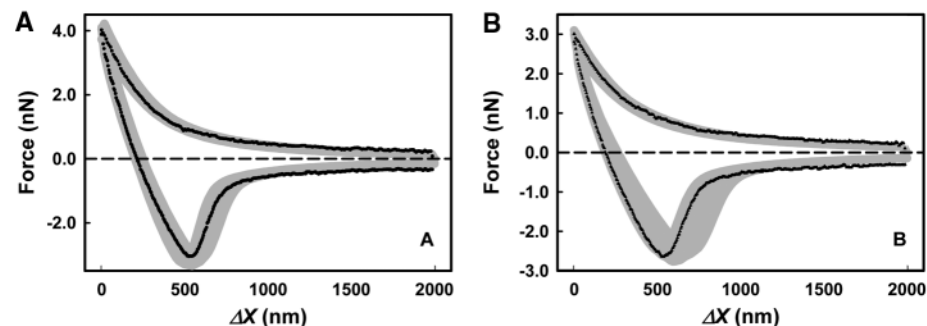


**Fig. 2.** The dynamic interaction force  $F$  versus piezo drive motion  $\Delta X$  between two decane droplets in aqueous solution in the presence of SDS at approach and retract velocities of 28  $\mu\text{m/s}$  at (A) 3 mM and (B) 10 mM SDS concentrations. The gray region represents the impact of the uncertainties in the theoretical calculations from independently measured parameters required for the calculations compared with the experimental data (points) plotted on the same graph.

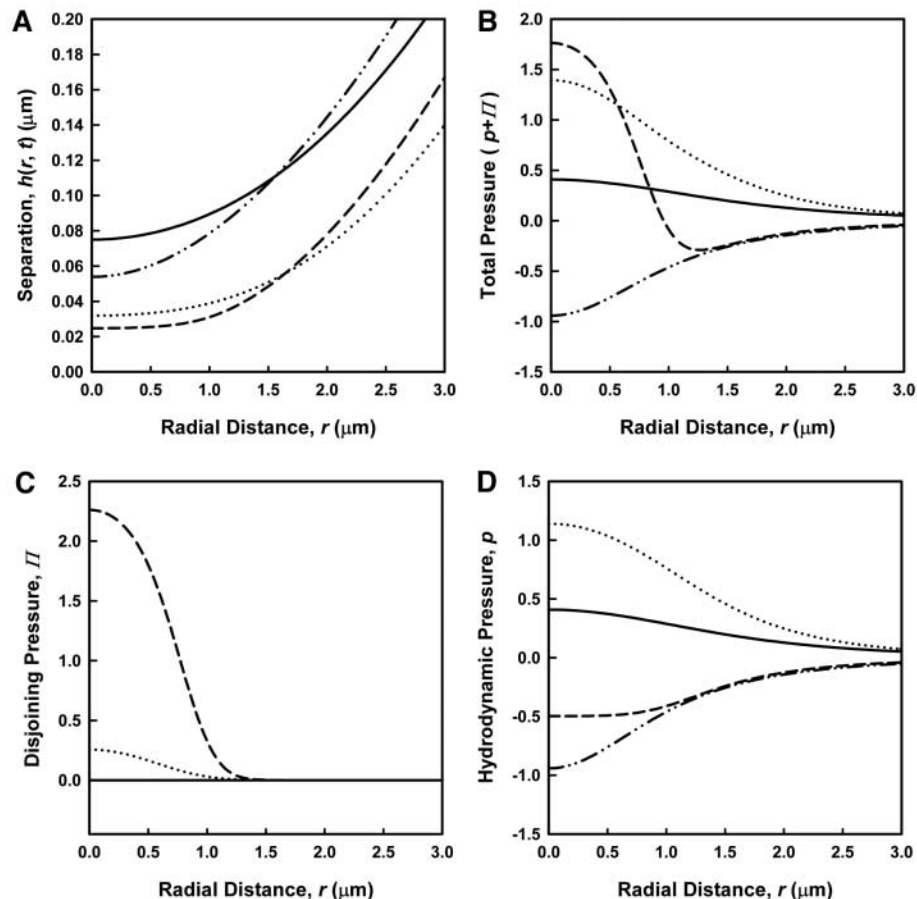


**Fig. 3.** Model calculations of droplet and pressure profiles for the 9.3  $\mu\text{m/s}$  approach and retract velocity for 0.1 mM SDS concentration at four times,  $t_1$  through  $t_4$ , in a 430.2-ms measurement. The four times are  $t_1 = 199.6$  ms (solid line),  $t_2 = 215.1$  ms (dotted line),  $t_3 = 223.7$  ms (dashed line), and  $t_4 = 240.9$  ms (dotted and dashed line). (A) The interfacial separation  $h$  as a function of radial distance  $r$ . (B) The total pressure between the droplets as a function of radial distance. Pressure is in dimensionless units, scaled by  $\sigma/R_0$ . (C) The disjoining pressure,  $\Pi$ , from only the equilibrium or static forces between the droplets as a function of radial distance. (D) The pressure  $p$  from only the hydrodynamic drainage effects as a function of radial distance.

from either equilibrium surface forces or hydrodynamic drainage. This is shown in Fig. 3A for the 10 mM SDS case at a series of times in the measurement conducted at a speed of 9.3  $\mu\text{m/s}$ . The interdroplet separation in Fig. 3A flattens at the time closest to the largest repulsive force, marked  $t_2$ , 215.1 ms into a 430.2-ms measurement. The total pressure in Fig. 3B is a combination of the component contributions shown in Fig. 3, C and D. The strong positive pressure in Fig. 3B at time  $t_2$  corresponds to the flat region in the interface profile in Fig. 3A.

The closest approach for the entire dynamic interaction event occurs in the retraction as shown at time  $t_3$ , 223.7 ms. The total radial pressure profile exhibits more features than any other curve in the time sequence in Fig. 3B, with a reversal from positive pressure at small radii to negative pressure at larger radii. This is due to the combination of pressure with different length scales from a positive equilibrium surface force at these interfacial separations and the negative hydrodynamic drainage pressure, as shown in Fig. 3, C and D. In contrast to the case involving only equilibrium interactions, for the dynamic interaction situation the closest approach, and hence opportunity for droplet coalescence to occur, can take place as the droplets move apart.

Ultimately it is clear that at velocities similar to those experienced through the Brownian motion of these droplets in solution, the contributions from hydrodynamic and surface forces are strongly coupled, and the relative length scales of these forces will influence which component dominates the interaction. The absence of a dimple in the interfacial profile when compared to drainage studies for larger droplets (12, 14, 20, 23, 24) is a product of both smaller droplet size and low deformation. The control of the velocity and interfacial tension in the experiment allows one to vary the relative effects so as to probe the situation where either surface force or hydrodynamic drainage can dominate the interactions behavior. For example, at even higher velocities, about twice those of the Brownian motion, the interfacial profile looks similar, but the contribution to the total pressure is then dominated by hydrodynamic drainage.

The thinning of the film in the radial center between the droplets at higher forces creates a remarkable coupling of the motion of the two droplets, which enhances the development of the smoothly varying minimum in the retract curve. The droplet velocity as a function of time at the axial and the edge positions of the droplet on the cantilever, for the 10 mM SDS concentration at 28  $\mu\text{m/s}$ , is shown in fig. S2. As the two droplets approach, the displacement of the center of the interface slows as the film thins, and the two interfaces become stationary for small radial distances near the turnaround point. The axial center of the top droplet continues to lag behind the motion of the rest of the droplet, even at the beginning of the retract motion. The axial center of the top droplet then decouples its motion from

the other droplet and accelerates to a velocity faster than the piezo drive with a recoiling motion before returning to rest. This behavior is described in the validated model without invoking interfacial rheological effects.

The agreement between the experimental data and the quantitative model identifies a number of important points related to describing interaction dynamics in liquid-liquid systems. This agreement is achieved by using the traditional no-slip boundary condition. This is contrary to what might be expected on the basis of some experimental observations of liquid drainage between rigid hydrophobic surfaces. One possible explanation is that the surface roughness of the oil-water interface is much smaller than that on a rigid surface, where deviations between theory and experiments have led to a heuristic correction to drainage models, referred to as a slip length. The quantitative visualization of the interfacial and pressure profiles provides a means of understanding the dynamic contributions from individual components in the physics of the interactions. The behavior of the droplet profile, pressure, and velocity upon the retraction presents an opportunity to probe systems possessing interfacial rheological characteristics and the impact of these on dynamic droplet-droplet interactions.

#### References and Notes

1. R. J. Hunter, *Foundations of Colloid Science* (Clarendon, Oxford, 1995).
2. J. N. Israelachvili, *Intermolecular and Surface Forces* (Academic Press, New York, 1992).
3. W. B. Russel, D. A. Saville, W. R. Schowalter, *Colloidal Dispersions* (Cambridge Univ. Press, New York, 1989).
4. H.-J. Butt, *J. Colloid Interface Sci.* **166**, 109 (1994).
5. W. A. Ducker, Z. G. Xu, J. N. Israelachvili, *Langmuir* **10**, 3279 (1994).

6. P. Mulvaney, J. M. Perera, S. Biggs, F. Grieser, G. W. Stevens, *J. Colloid Interface Sci.* **183**, 614 (1996).
7. D. E. Aston, J. C. Berg, *Ind. Eng. Chem. Res.* **41**, 389 (2002).
8. R. R. Dagastine, G. W. Stevens, D. Y. C. Chan, F. Grieser, *J. Colloid Interface Sci.* **273**, 339 (2004).
9. S. L. Carnie, D. Y. C. Chan, C. Lewis, R. Manica, R. R. Dagastine, *Langmuir* **21**, 2912 (2005).
10. S. L. Carnie, D. Y. C. Chan, R. Manica, *ANZIAM J.* **46(E)**, C808 (2005).
11. I. Ivanov, D. Dimitrov, *Surfact. Sci. Ser.* **29**, 379 (1988).
12. S. Abid, A. K. Chesters, *Int. J. Multiphase Flow* **20**, 613 (1994).
13. S. G. Yiantsios, R. H. Davis, *J. Fluid Mech.* **217**, 547 (1990).
14. A. K. Chesters, *Chem. Eng. Res. Des.* **69**, 259 (1991).
15. S. A. Nespolo, M. A. Bevan, D. Y. C. Chan, F. Grieser, G. W. Stevens, *Langmuir* **17**, 7210 (2001).
16. D. Bhatt, J. Newman, C. J. Radke, *Langmuir* **17**, 116 (2001).
17. D. Y. C. Chan, R. R. Dagastine, L. R. White, *J. Colloid Interface Sci.* **236**, 141 (2001).
18. R. R. Dagastine, T. T. Chau, D. Y. C. Chan, G. W. Stevens, F. Grieser, paper presented at the 7th World Congress of Chemical Engineering, Glasgow, Scotland, 10–14 July 2005.
19. J. C. Baygents, D. A. Saville, *J. Chem. Soc. Faraday Trans.* **87**, 1883 (1991).
20. E. Klaseboer, J. P. Chevallier, C. Gourdon, O. Masbernat, *J. Colloid Interface Sci.* **229**, 274 (2000).
21. Materials and methods are available as supporting material on Science Online.
22. J. L. Hutter, J. Bechhoefer, *Rev. Sci. Instrum.* **64**, 1868 (1993).
23. J. N. Connor, R. G. Horn, *Faraday Discuss.* **123**, 193 (2003).
24. D. G. Goodall, M. L. Gee, G. Stevens, J. Perera, D. Beaglehole, *Colloids Surf. A* **143**, 41 (1998).
25. This work was supported by the Australian Research Council and by the National Science Foundation under Grant No. INT-020267.

#### Supporting Online Material

www.sciencemag.org/cgi/content/full/313/5784/210/DC1  
Materials and Methods  
Figs. S1 and S2

30 January 2006; accepted 1 June 2006  
10.1126/science.1125527

## Tyrannosaur Life Tables: An Example of Nonavian Dinosaur Population Biology

Gregory M. Erickson,<sup>1\*</sup> Philip J. Currie,<sup>2</sup> Brian D. Inouye,<sup>1</sup> Alice A. Winn<sup>1</sup>

The size and age structures for four assemblages of North American tyrannosaurs—*Albertosaurus*, *Tyrannosaurus*, *Gorgosaurus*, and *Daspletosaurus*—reveal a pronounced, bootstrap-supported pattern of age-specific mortality characterized by relatively high juvenile survivorship and increased mortality at midlife and near the maximum life span. Such patterns are common today in wild populations of long-lived birds and mammals. Factors such as predation and entrance into the breeding population may have influenced tyrannosaur survivorship. This survivorship pattern can explain the rarity of juvenile specimens in museum collections.

Little is known about the population biology of nonavian dinosaurs. Did these animals show survivorship patterns akin to extant living dinosaurs—the birds, like the dinosaurs' cousins the crocodylians, or were they similar to more distantly related ecological analogs? Here, we use the age and size distribution from a death assemblage of the North American tyrannosaur *Albertosaurus*

*sarcophagus* to produce an age-standardized ecological life table for a nonavian dinosaur population.

<sup>1</sup>Department of Biological Science, Florida State University, Tallahassee, FL 32306, USA. <sup>2</sup>Department of Biological Sciences, University of Alberta, Alberta T6G 2E, Canada.

\*To whom correspondence should be addressed. E-mail: gerickson@bio.fsu.edu

## Supporting Online Material

### Materials and Methods

A Digital Instruments Multimode AFM, Nanoscope IIIa AFM controller, and commercially available fluid cell and o-ring were used for all experiments. Silica nitride contact cantilevers (Veeco Metrology) were sputter coated with 1 nm of chromium and then 10 nm of gold, and then hydrophobized according to (S1). Cantilever spring constant was 0.12 N/m, measured according to the method of (S2). The bottom substrate was a nitric acid cleaned glass slide, sputtered coated with 1 nm of chromium and 20 nm of gold and then hydrophobized as above. The droplet was immobilized on the bottom substrate according to the method developed in (S3). The droplet was attached to the cantilever in aqueous solutions of sodium dodecyl sulfate (BDH Laboratory Supplies, SDS) using a step motor controlled syringe (World Precision Instruments, Inc.) injecting nanoliter volumes of n-decane (Aldrich chemical) through a glass capillary (inner diameter  $\sim 10 \mu\text{m}$ ). All solutions contained a background electrolyte of 1 mM sodium nitrate. The SDS concentrations were changed in situ where each solution was given 30 minutes to thermally equilibrate before any data were taken. The oil droplets were positioned first using the course stepping motor, and then using the piezo tube fine control. The force curves (an approach and retract force-distance cycle) were taken at a series of scan rates at eight different approach speeds varying from  $2 \mu\text{m/s}$  to  $28 \mu\text{m/s}$ . Force curves were measured between the droplets at SDS concentrations of 0.1, 1.0, 3.0, and 10 mM. At the end of the experiments, the droplets were flushed from the system and force curves between the substrate and cantilever were recorded to determine the detector sensitivity of the AFM photodiode. The undistorted radii of the droplets on the cantilever and the substrate were estimated to be  $43 \mu\text{m} \pm 2 \mu\text{m}$  and  $90 \mu\text{m} \pm 2 \mu\text{m}$ , respectively, from CCD camera measurements. The AFM photodiode voltage was converted to cantilever deflection using the detector sensitivity determined at the end of the experiment and then converted to force via  $F = k_c \Delta d$ , where  $k_c$  is the spring constant of the cantilever.

Interfacial tension was measured using the pendent droplet method with a DataPhysics OCA 20 Tensiometer and axisymmetric droplet shape analysis software. The interfacial tension for this system is also well characterized and ranges from 39 mN/m to 8 mN/m(S4). Sessile droplet contact angle measurements of decane droplets on the glass substrate in aqueous surfactant solutions were made using the same system. The contact angle of the droplet on the piezo drive was determined from this macroscopic contact angles, approximately  $50^\circ$ , whereas the cantilever droplet is treated with a pinned contact line on the sharp edge of the cantilever with a droplet contact angle of approximately  $130^\circ$ .

The model requires that the time scale of the droplet response to deformation must be much faster than the time scale of the approach speed of two droplets(S5). In addition the hydrodynamic model employs new boundary condition at large  $r$  distances derived from the constant volume constraint for the droplets given (S5) by:

$$\dot{h} + \left( F_1 + F_2 - \frac{2\pi\sigma}{k_c} \right) \dot{G} = \mp V \quad \text{for } r = r_{\max} \quad [\text{S1}]$$

where  $k_c$  is the cantilever spring constant and  $G$  and  $F_i$  are defined as

$$G = \frac{F}{2\pi\sigma} = \frac{1}{\sigma} \int_0^{\infty} r[p(r,t) + \Pi(h(r,t))]dr \quad F_i = 1 + \frac{1}{2} \ln\left(\frac{r_{\max}^2}{4R_i^2}\right) + \frac{1}{2} \ln\left(\frac{1 + \cos\theta_i}{1 - \cos\theta_i}\right) \quad [\text{S1}]$$

where  $G$  is an integral over the product of pressure and the interfacial profile and  $F_i$  is a function of contact angle,  $\theta_i$ , and radii,  $R_i$ , of each droplet. The numerical calculation of the hydrodynamic drainage model using the above boundary condition employs the methods of lines and the central difference method to construct a system of differential algebraic equations(S5).

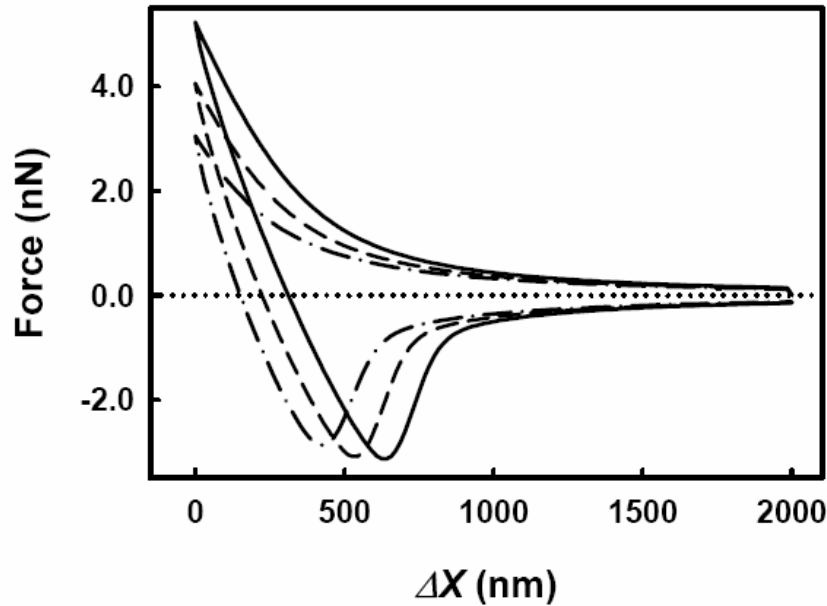


Fig. S1. Force profiles the approach and retract velocity is  $V = 28\mu\text{m/s}$  and the ionic strength is matched to the 3 mM SDS case for three different starting positions,  $h_0 = 1.67\ \mu\text{m}$  (solid line),  $1.77\ \mu\text{m}$  (dashed line) and  $1.87\ \mu\text{m}$  (dash-dot line). The electrostatic double layer surface potential was  $-100\ \text{mV}$ , and the piezo displacement, cantilever spring constant, droplet radii, contact angle and interfacial tension matched the experimental conditions for the 3 mM SDS measurement.

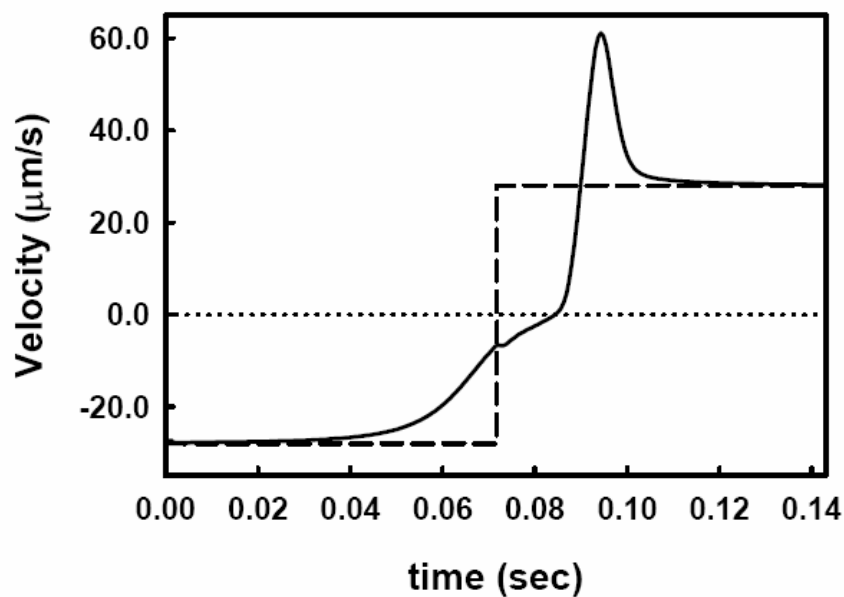


Fig. S2. Velocity as a function of time at the axial position (solid line) of the droplet and the piezo drive velocity (dashed line) for the approach and retract traces of the force curve for 28  $\mu\text{m/s}$  at an SDS concentration of 10 mM.

### References and Notes

- S1. J. L. Hutter, J. Bechhoefer, *Rev. Sci. Instrum.* **64**, 1868 (1993).
- S2. J. F. Wall, F. Grieser, C. F. Zukoski, *J. Chem. Soc., Faraday Trans.* **93**, 4017 (1997).
- S3. R. R. Dagastine, D. C. Prieve, L. R. White, *J. Colloid Interface Sci.* **269**, 84 (2004).
- S4. S. A. Nespolo, M. A. Bevan, D. Y. C. Chan, F. Grieser, G. W. Stevens, *Langmuir* **17**, 7210 (2001).
- S5. S. L. Carnie, D. Y. C. Chan, C. Lewis, R. Manica, R. R. Dagastine, *Langmuir* **21**, 2912 (2005).